Theoretical Investigations of Mode Mixing in Vibrationally Excited States of CH_5^+ †

Charlotte E. Hinkle and Anne B. McCoy*

Department of Chemistry, The Ohio State University, Columbus, Ohio 43210

Received: December 20, 2008; Revised Manuscript Received: February 9, 2009

Using diffusion Monte Carlo, five vibrational excited states of CH_5^+ and CD_5^+ are evaluated and analyzed. Here, we focus on the fundamentals in the five modes that are generated by requiring that the wave functions change sign at specified values of the five symmetry-adapted linear combinations (SALCs) of the CH or CD bond lengths. Even though the definitions of these modes are based on displacements of the CH or CD bond lengths, the frequencies are found to be low compared to previously calculated CH vibrational frequencies in this molecule. The totally symmetric mode, with A_1^+ symmetry, has a calculated frequency of 2164 and 1551 cm^{-1} for CH_5^+ and CD_5^+. The frequencies of the four fundamentals that arise from excitation of the four SALCs that transform under G_1^+ symmetry have frequencies that range from 1039 to 1383 cm^{-1} and from 628 to 893 cm^{-1} in CH_5^+ and CD_5^+, respectively. The origins of the broken degeneracy are investigated and explained to reflect extensive coupling to the two low-frequency modes that lead to isomerization of CH_5^+.

1. Introduction

Protonated methane has intrigued and challenged theorists and spectroscopists since it was first detected by mass spectrometry.[1] It is of particular interest to astrochemists, as it is believed to be an intermediate in the reaction of H_2 with CH_3^+.[2–4] This reaction is thought to be responsible for the nonstatistical hydrogen/deuterium isotopic fractionation in partially deuterated CH_3^+ in the interstellar medium. Whether CH_5^+ exists as a stable long-lived species in dense interstellar clouds remains an open issue. The challenge in answering this question comes from the absence of an assigned high-resolution spectrum. Such a spectrum would provide the signatures of CH_5^+ that are required to identify its presence and abundance in interstellar spectra.

The absence of an assigned spectrum reflects challenges both in obtaining a rotationally resolved, high-resolution spectrum and in assigning the peaks to transitions between specific rotation−vibration energy levels. Two spectra have been reported in the region of the CH stretch fundamental. Nearly 10 years ago, Oka and co-workers[5] reported the first high-resolution spectrum of CH_5^+. At that time, no assignments were made. More recently, a lower-temperature spectrum was obtained by Savage, Dang, and Nesbitt.[6] Although patterns have been identified in this spectrum and some assignments have been made, much of the spectrum remains unassigned.[7] In addition, a third, low-resolution, laser-induced-reaction (LIR) spectrum was reported by Asvany et al.[8] Although this spectrum does not provide the signatures needed to identify CH_5^+ within the interstellar spectrum, it does provide an overall contour of the spectrum for frequencies above 1000 cm^{-1}.

Why should the infrared spectrum of a molecule that consists of six atoms, five of which are hydrogen atoms, be so difficult to understand? According to calculations performed at the CCSD(T)/aug-cc-pvtz level, the dissociation energy of CH_5^+ to form $CH_3^+ + H_2$ is 47 kcal/mol,[9] making CH_5^+ a reasonably strongly bound molecular ion. On the other hand, close examination of the potential surface below 350 cm^{-1} reveals a surprisingly flat potential. By symmetry, the potential surface that describes CH_5^+ must have 120 energetically equivalent minima. These correspond to the 120 ways in which five atoms can be bound to a single central atom. The minimum-energy geometry of CH_5^+ is depicted in the left and right columns of Figure 1. At these stationary points, the molecule has C_s symmetry, and these stationary points are often collectively referred to as the C_s(I) minimum. The 120 equivalent minima are connected by a chain of saddle points that are represented by the structures in the central column of Figure 1. The lower-energy saddle point also has C_s symmetry and is referred to as the C_s(II) saddle point. It has an energy approximately 30 cm^{-1} above the C_s(I) minimum.[9] There are 120 energetically equivalent saddle points with this structure.[10–13] The other low-lying saddle point has C_{2v} symmetry and an energy that is approximately 340 cm^{-1} above the global minimum.[9] There are 60 equivalent C_{2v} saddle points[10–13] on the global surface for CH_5^+. Taking these 180 saddle points into account, one can find a path that connects any of the C_s(I) minima to any of the other 119 minima.

Because motion across these saddle points primarily involves the hydrogen atoms and the saddle points all have energies below 350 cm^{-1}, it is not surprising that the ground-state wave function has significant amplitude in all of the minima, as well as the saddle points that connect the minima.[14–17] This observation was supported by the recent work of Wang and Carrington[18] in which they performed large-scale variational calculations on CH_5^+. They found that energy level patterns for the bending modes were not significantly affected when they replaced the potential surface of Jin et al. by one in which any electronic energy below 2000 cm^{-1} was replaced with an energy value of 2000 cm^{-1}. This and earlier studies point to an image in which CH_5^+ freely isomerizes among the 120 equivalent minima in the potential.[17,19–22] To date, a model Hamiltonian that fully captures the large-amplitude motions in CH_5^+ has not been developed. This makes the assignment of the high-resolution spectrum a challenge.

† Part of the "George C. Schatz Festschrift".

* To whom correspondence should be addressed. E-mail: mccoy@chemistry.ohio-state.edu.

10.1021/jp8112733 CCC: $40.75
Published on Web 03/16/2009

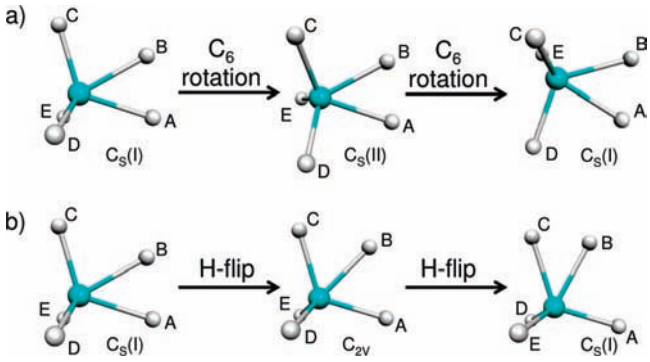

Figure 1. Geometries of CH_5^+ at the three lowest-energy stationary points. In the left and right columns, the C_s(I) minimum structures are shown. In the center column, the transition states with (a) C_s and (b) C_{2v} symmetry that connect these minima are depicted. The letters on each structure are used to identify the locations of particular hydrogen atoms in the CH_5^+ molecular ion.

To investigate how the delocalization of the wave function among such a large number of equivalent minima is affected by vibrational excitation and how this is reflected in the spectrum, we have embarked on a series of studies in which we probe vibrationally and rotationally excited states of CH_5^+ using quantum Monte Carlo techniques.[23,24] Within this approach, we generate excited states by requiring that the wave function changes sign at selected molecular geometries. This approach generally does not produce molecular eigenstates. Instead, it produces the lowest-energy zero-order states that have the required properties, for example, a state in which the wave function changes sign as the CH bond lengths are extended.

In this study, we draw from the high symmetry of CH_5^+ and investigate the nature of vibrationally excited states obtained by putting one quantum of excitation in the vibrational modes that are generated by taking the linear combinations of the CH bond lengths that transform as A_1^+ or G_1^+ under the G_{240} permutation-inversion symmetry group for CH_5^+.[25] For comparison, we have also studied how complete deuteration affects these results by calculating the same set of excited states for CD_5^+. It should be noted that, although the nodal structure that we have chosen depends on the values of the CH or CD distances, the fact that diffusion Monte Carlo (DMC) will generate the *lowest-energy* state with the chosen symmetry properties does not ensure that the states we access will be CH stretch fundamentals. Rather, by analyzing the delocalization (or localization) of the probability amplitudes associated with the ground and excited states among the 120 equivalent minima on the potential surface, we are able to gain insights into the nature of the couplings within CH_5^+.

2. System

Before discussing the methods used in this study, it is useful to review some of the properties of CH_5^+. Whereas the ground state has equal probability amplitude in all 120 minima, some of the excited states do not. This assertion reflects the fact that the full permutation-inversion symmetry of CH_5^+ (G_{240}) is much higher than the point-group symmetry of any of the stationary points that are sampled by the ground-state wave function (C_{2v}). Similar behavior is seen in molecules, such as methanol, that have a 3-fold torsion barrier. In Figure 2, we plot a one-dimensional potential of this form, as well as the probability amplitude associated with the three lowest-energy eigenstates. As can be seen, the ground state (plotted in black) has equal amplitudes in all three wells, whereas the other two states

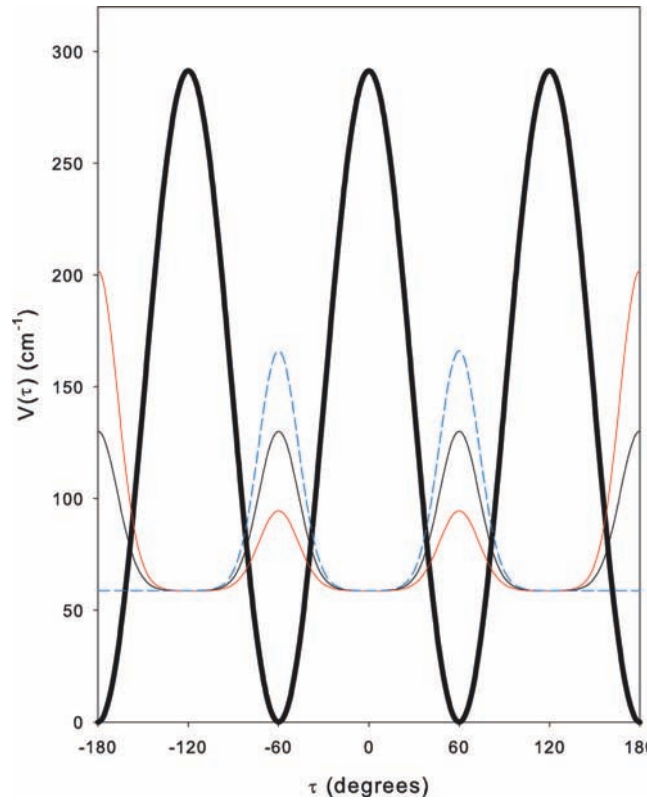

Figure 2. Potential (thick black line) and probability amplitudes (thin lines) associated with the three lowest-energy wave functions for a 3-fold torsion barrier. The state plotted in black is the ground state. The other two states make up the doubly degenerate first excited state. The parameters used for this calculation were based on a study of the methyl rotor in CH_3O_2.[26]

(plotted in red and blue) have equal amplitudes in the two central wells but either zero or more amplitude in the outer wells. Similar behavior is expected for degenerate levels in CH_5^+. This being the case, it will also be useful to find methods for dividing the probability amplitude into 120 pieces, each of which is assigned to a single potential minimum.

As mentioned above, there are three important low-energy stationary points on the CH_5^+ potential. All are depicted in Figure 1 and have calculated energies that are below 350 cm^{-1}.[9] On average, all five CH bonds are equivalent. In examining the CH and HH bond lengths at the three stationary points, the equivalence is less obvious. As the bond lengths reported in Table 1 indicate, in the two structures with C_s symmetry, the r_{AB} distance is only 0.95 Å, based on CCSD(T) calculations.[9,27] These two hydrogen atoms are also associated with CH distances that are longer than the other three CH bond lengths by about 0.01 Å. Based on these and other considerations,[17,24,27] the two hydrogen atoms that are closest together in the two structures with C_s symmetry are referred to as the H_2 subunit, and the remaining three hydrogen atoms along with the carbon atom are referred to as the CH_3^+ subunit. Motion across the C_s(II) saddle point corresponds to a 60° rotation of the CH_3^+ subunit and is shown in Figure 1a. The motion across the C_{2v} saddle point corresponds to exchange of a hydrogen between the two subunits and is shown in Figure 1b.

Based on these considerations, we have developed an approach that allows us to assign an arbitrary molecular geometry to a specific minimum on the potential. This requires that we label the five hydrogen atoms in an arbitrary structure of CH_5^+ so that they correlate to the labels in Figure 1. The

TABLE 1: CH and HH Bond Lengths[a] (Å) at the Three Stationary Points[b]

	structure		
bond	C_s(I)	C_s(II)	C_{2v}
CH_A	1.20	1.20	1.14
CH_B	1.20	1.20	1.16
CH_C	1.11	1.10	1.14
CH_D	1.09	1.10	1.09
CH_E	1.09	1.08	1.09
H_AH_B	0.95	0.94	1.18
H_AH_C	2.04	2.02	2.00
H_AH_D	1.72	1.55	1.75
H_AH_E	1.72	1.84	1.75
H_BH_C	1.44	1.55	1.18
H_BH_D	1.94	2.02	1.94
H_BH_E	1.94	1.84	1.94
H_CH_D	1.79	1.76	1.75
H_CH_E	1.79	1.85	1.75
H_DH_E	1.88	1.85	1.81

[a] Reference 9. [b] See Figure 1.

hydrogen atoms that make up the H_2 subunit are identified as H_A and H_B, and the hydrogen atoms labeled C−E make up the CH_3^+ subunit. We then chose the B and C labels by requiring that the distance between these two atoms be the shortest of the six possible hydrogen−hydrogen distances that involve one hydrogen atom from each subunit. The atoms labeled D and E are chosen to satisfy the requirement that hydrogen atoms C−E contained within the CH_3^+ subunit are oriented in a clockwise manner. Although this is shown for the three stationary-point geometries in Figure 1, this approach can be applied to any arbitrary molecular geometry.

3. Theory

3.1. Diffusion Monte Carlo. For this study, we use diffusion Monte Carlo (DMC) to obtain both the energy and wave functions for the ground and selected excited states of CH_5^+. As these approaches are discussed elsewhere,[28−30] we discuss them only briefly here. In addition, the parameters used for the present study of CH_5^+ are identical to those used in our earlier study, and the reader is referred to ref 24 for the specific numerical details.

The DMC approach is a statistical method for solving the time-dependent Schrödinger equation at long imaginary times, τ, where

$$\tau = \frac{it}{\hbar} \tag{1}$$

and the wave function is represented by an ensemble of δ-functions, which are often referred to as walkers. At long imaginary times, the distribution of walkers provides a Monte Carlo sampling of the wave function for the state of interest. The descendant weighting technique is used to obtain the associated probability amplitude,[30,31] which can be used to obtain expectation values of multiplicative operators or projected onto any coordinate or coordinates of interest.

In this study, we use the global potential surface for CH_5^+, developed by Jin et al.[9] To account for the equivalence of the minima, our DMC algorithm is modified slightly to ensure that the wave function has the proper symmetry. Specifically, at each time step, the coordinates of a randomly selected pair of fungible hydrogen atoms are exchanged. In principle, this should not be necessary, but we and others have found that, when there is an effective barrier between minima that is large enough that there is zero-probability amplitude in the classically forbidden region of the potential, the distribution of walkers can become localized in a subset of the minima.[32] This addition to our algorithm prevents this from occurring and has no effect on the resulting energies, within the statistical uncertainties of the simulation.

The focus of the present study is on vibrationally excited states of CH_5^+, and we use the fixed-node treatment, originally described by Anderson, to evaluate these energies and wave functions.[29] Nodal surfaces divide the wave function into two pieces for which the amplitude is either positive or negative throughout. Near the node, the wave function approaches zero with a finite slope. This behavior is identical to that of a wave function near an infinite potential barrier. As such, within the fixed-node treatment, configuration space is divided into two parts, using the nodal surface as the dividing surface. The region of space in which the amplitude of the wave function is positive is denoted r_+, and the remaining region of space is denoted r_-. As such, the fixed-node calculations are performed in two parts. In one, the global potential for CH_5^+ is used for r_+, and the potential is made to be infinite in r_-. In the second, the regions are reversed. Because the amplitude of the wave function must be zero in regions of infinite potential energy, any walker that attempts to cross from r_+ to r_- will be removed from the ensemble. Further, because $\Delta\tau$ is finite, a recrossing correction needs to be introduced.[29] This correction depends exponentially on the product of the distance of the walker from the node before and after a displacement to the mass associated with this motion. As we are considering nodal surfaces that depend on a single coordinate, the appropriate mass is given by the reciprocal of the Wilson G-matrix element associated with the nodal coordinate.[33] As the energies associated with the two simulations should be equal, a check on the functional form of the nodal surface is provided by calculating the differences between these two energies. If it is statistically nonzero, the node has not been properly placed.

A challenge in implementing the fixed-node treatment comes in the definition of the nodal surface. For the present study, we require that the wave function change sign at a specified value of the various symmetry-adapted linear combinations of the CH or CD bond lengths, described below. This is straightforward to implement when the value of the coordinate at the node can be determined to be zero, by symmetry. Complications arise for determining the position of the node in excitations along totally symmetric coordinates. In this case, we implement a modified version of the fixed-node approach in the form of adiabatic diffusion Monte Carlo (ADMC).[34,35] This approach provides a way to determine the optimal position of the nodal surface, as well as the associated excited-state energy.

Once the simulations have been run, we have two separate wave functions, one with positive amplitude and one with negative amplitude. The full wave function is obtained by splicing these two pieces together. This introduces an additional challenge. Because the simulations that generated the two parts of the wave function are performed independently, one must determine the relative weights of the two pieces. Several approaches have been proposed for doing this.[36] One possibility is to require that the excited state be orthogonal to the ground state.[37] A second approach, discussed by Sandler et al.,[38] introduces the requirement that the slope be continuous across the node. We employ a modification of the second approach, requiring the second derivative of the probability amplitude to be continuous across the node. The challenge in this approach is that we are dealing with a $3N$-dimensional representation of the wave function, whereas the nodal surface is $(3N - 1)$-dimensional. If we project the probability amplitude onto the coordinate along which the wave function changes sign, the problem becomes tractable.

3.2. Symmetry Coordinates. As alluded to above, in this study, we examine the vibrationally excited states of CH_5^+, defined

TABLE 2: Identification of the Unique Sets of Minima for Each of the Four Excited States along the G_1^+ Modes[a]

mode	number of equivalent minima	positive[b]	negative[c]	near zero[d]	zero probability[e]
$q_{G_1^+,1}$[f]	6	4XXX5, X45XX X4XX5, X4X5X 4X5XX, 4XX5X	5XX4X, X54XX 5X4XX, X5XX4 X5X4X, 5XXX4	XX4X5, XX5X4 XX54X, XX45X	45XXX, 54XXX XXX54, XXX45
$q_{G_1^+,2}$[g]	4	3XYYX, X3XYY 3XYXY, X3YYX 3XXYY, X3YXY	YYXX3, YYX3X YY3XX	Y3XYX, Y3XXY YX3YX, XYYX3 YX3XY, XX3YY	3YXYX, Y3YXX 3YYXX, 3YXXY XYXY3, YXY3X XY3XY, XXYY3 XY3YX, XXY3Y YXX3Y, YXYX3 XYX3Y, YXXY3
$q_{G_1^+,3}$[h]	6	12XXX, 21XXX	XX1X2, XXX21 XX21X, XX12X XXX12, XX2X1	X21XX, 1XX2X 1XXX2, X12XX	2XXX1, X1X2X 1X2XX, X1XX2 X2X1X, 2X1XX 2XX1X, X2XX1
$q_{G_1^+,4}$[i]	24	X1XXX, 1XXXX	XXX1X, XXXX1 XX1XX	–	–

[a] Number labels identify positions of unique hydrogen atoms, with the five positions corresponding to ABCDE, as described in the text. [b] Populated minima in the region where $q_{G_1^+,n} > 0$. [c] Populated minima in the region where $q_{G_1^+,n} < 0$. [d] Minima less than 10% of the amplitude of the most populated minimum. [e] Minima less than 1% of the amplitude of the most populated minimum. [f] X = H_1, H_2, or H_3. [g] X = H_1 or H_2 and Y = H_4 or H_5. [h] X = H_3, H_4, or H_5. [i] X = H_2, H_3, H_4, or H_5.

as the symmetry-adapted linear combinations (SALCs) of the CH bond lengths that transform as A_1^+ or G_1^+ under the G_{240} complete nuclear permutation-inversion (CNPI) group. A CNPI group is defined by all of the permutations of a given set of like nuclei. The group is of order $\prod_i n_i!$ to account for all of the permutations of each of the sets of n_i identical nuclei in the molecule.[25] The number of permutations is then multiplied by 2 to account for inversion. In the case of CH_5^+, there are five hydrogen atoms and one carbon atom, so the CNPI group has 240 = 5!1!2 elements. The character table for the G_{240} group is provided in the Supporting Information.

Based on this character table, the symmetry-adapted linear combinations of the five CH or CD stretches transform under G_1^+ and A_1^+ and are defined as

$$q_{A_1^+} = \sqrt{\frac{1}{5}}(r_1 + r_2 + r_3 + r_4 + r_5) \quad (2)$$

$$q_{G_1^+,1} = \sqrt{\frac{1}{2}}(r_4 - r_5) \quad (3)$$

$$q_{G_1^+,2} = \sqrt{\frac{1}{6}}(2r_3 - r_4 - r_5) \quad (4)$$

$$q_{G_1^+,3} = \sqrt{\frac{1}{12}}(3r_2 - r_3 - r_4 - r_5) \quad (5)$$

$$q_{G_1^+,4} = \sqrt{\frac{1}{20}}(4r_1 - r_2 - r_3 - r_4 - r_5) \quad (6)$$

where r_j represents the distance between the carbon atom and the jth hydrogen atom. In these definitions of the excited states of G_1^+ symmetry, the five hydrogen atoms are no longer equivalent, and in the permutation algorithm, described above, only equivalent hydrogen atoms are permuted. For example, in the case of the state with excitation in $q_{G_1^+,1}$, the hydrogen atoms labeled 4 and 5 are not equivalent to any of the others, but the three remaining hydrogen atoms, those labeled 1−3, remain equivalent. As such, only permutations among the three equivalent hydrogen atoms are considered. As a result, the 120 equivalent minima can be subdivided into 20 groups of 6 each. The probability amplitudes in minima in the same group must be equal.

The above discussion implies a loss of symmetry in some excited states, and this might be surprising. If one considers the plots of the eigenstates of the one-dimensional potential (Figure 2), one immediately sees that the probability amplitudes that arise from the two states with E symmetry, plotted in red and blue, do not have equal amplitudes in all three wells. It is this factor that we are capturing in our permutation algorithm. Even in the absence of the permutation, we will find different populations of walkers in different potential minima. The permutation approach attempts to remove differences in the populations that are due to statistics as opposed to differences that reflect the physics of the system. In the end, the energies of the calculated states are not affected by the introduction of permutation.

In the discussion that follows, we identify minima based on the locations of the unique atoms using a five-character string indicating which of the five hydrogen atoms is in the positions labeled A−E. When a hydrogen atom is unique by symmetry, its atom number is used to denote its position, as in the case of H_4 and H_5 in the example above. When two or more hydrogen atoms are equivalent by symmetry, their identities are represented by the letter X or Y. In the example above, X could represent H_1, H_2, or H_3. Table 2 provides a list of all distinct minima, based on the definition of the four modes that transform under G_1^+ in eqs 3−6.

3.3. Analysis Techniques. One-dimensional probability distributions, rotational constants, and participation ratios are obtained from the calculated probability amplitudes. These quantities provide information that is essential for generating a picture of the structures that are sampled by CH_5^+ in the ground state and various excited states. As such, analysis of these quantities aids in our overall understanding of the dynamics of

CH_5^+. When analyzing the wave function, we use several techniques, as follows:

1. Projections of the Probability Amplitude. One-dimensional probability distributions are evaluated by projecting the probability amplitude onto a single coordinate. Following earlier work, the coordinates on which we focus are the CH and HH bond lengths and the two isomerization coordinates, ϕ and q. Here, q is the coordinate that connects two adjacent minima through a C_{2v} saddle point

$$|q| = |r_{H_BH_C} - r_{H_AH_B}| \tag{7}$$

and motion along ϕ corresponds to motion across a C_s(II) saddle point. Specifically, ϕ is defined as the angle between the vector along the CH_C, CH_D, or CH_E bond axis and the plane that contains H_A, H_B, and the carbon atom.[24]

2. Participation Ratios. The participation ratio, ρ, provides a measure of how many minima are populated in a given excited state. This quantity is defined as[39,40]

$$\rho = \frac{1}{\sum_{i=1}^{120} p_i^2} \tag{8}$$

where p_i represents the probability amplitude in the ith minimum. In the ground state, $p_i = 1/120$ for all i, and $\rho = 120$. For excited states, the minima will not necessarily contain equal probability amplitudes, and ρ provides a measure of how many minima are sampled in these states.

3. Rotational Constants. Rotational constants for the various excited states are calculated by first transforming the geometries of each of the walkers in the ensemble into an Eckart frame.[23,41,42] The precise definition of this frame depends on the choice of the static molecular model. With the high symmetry of CH_5^+ and the existence of three classes low-energy stationary points, there are a number of structures that could be used. For example, there are 120 geometries that correspond to each of the C_s(I) minima and 120 for each of the C_s(II) saddle points. Following our earlier work on isotopologues of CH_5^+,[23] we evaluate the rotational constants, using each of the 240 stationary points enumerated above, to define the static molecular model. Once the static molecular model is chosen, all of the walkers are rotated into an Eckart frame based on that choice. The rotational constants are evaluated as the expectation values of the elements of the inverse of the moment of inertia tensor, multiplied by the appropriate constants.

As described above, for some of the excited states, the probability amplitudes at the minima that correspond to the 120 C_s(I) static molecular models will not be equal. In collecting these data, we report the weighted averages of the 120 calculated rotational constants, weighting the values by p_i in eq 8. When a C_s(II) saddle-point structure is used for the static molecular model, we weight the individual rotational constants by the average populations in the minima that are connected by that saddle point. Again, the reported rotational constants represent the weighted averages of the results of the 120 separate calculations in each case.

4. Results

We use DMC to evaluate the energies, wave functions, and probability amplitudes of the lowest-energy states that have a single node along each of the five coordinates, defined in eqs 2−6. The resulting energies are reported in the third column of Table 3. There are two surprising features of these results.

TABLE 3: Excited-State Energies (cm^{-1}) for CH_5^+ and CD_5^+ [a]

node[b]	energy	ρ[c]
CH_5^+		
$q_{G_1^+,2} = 0$	1039 ± 5	32 ± 1
$q_{G_1^+,3} = 0.01527 \pm 0.00005$ Å	1150 ± 5	36 ± 1
$q_{G_1^+,1} = 0$	1172 ± 5	65 ± 5
$q_{G_1^+,4} = 0.01435 \pm 0.00004$ Å	1383 ± 5	108 ± 2
$q_{A_1^+} = 2.58790 \pm 0.00005$ Å	2160 ± 5	120
CD_5^+		
$q_{G_1^+,2} = 0$	628 ± 5	24 ± 1
$q_{G_1^+,3} = 0.01401 \pm 0.00007$ Å	716 ± 5	34 ± 1
$q_{G_1^+,1} = 0$	729 ± 5	60 ± 3
$q_{G_1^+,4} = 0.01328 \pm 0.00004$ Å	893 ± 5	104 ± 2
$q_{A_1^+} = 2.57435 \pm 0.00003$ Å	1551 ± 5	120

[a] Energies are reported relative to a zero-point energy of 10 916 ± 5 cm^{-1} for CH_5^+ and 8045 ± 5 cm^{-1} for CD_5^+. [b] Definition of the node used for the fixed-node DMC calculation. [c] Defined in eq 8.

First, the calculated energies are too low for these calculated states to be fundamentals in the CH stretching vibrations. This is particularly notable for the four states with nodes in the four $q_{G_1^+,n}$ coordinates. Even the fifth state, that in which the wave function is constrained to change sign at a specified value of the sum of the five CH distances, has an energy that is on the very low end of the frequency range for the CH stretch. In contrast, based on converged variational approaches, Wang and Carrington obtained frequencies for the two stretch fundamentals of CH_5^+ equal to 2467 cm^{-1} (G_1^+) and 2969 cm^{-1} (A_1^+).[18] Based on the large frequency differences, it appears that the fixed-node DMC calculations are not generating the CH stretch fundamentals. Rather, we are locating the lowest-energy state that has the property that the wave function changes sign at a specified value of one of the these linear combinations of the internal coordinates. Based on the frequencies, we believe that the states that are being sampled can be better described as combinations of HCH bends and the two low-frequency isomerization coordinates than as CH stretches.

This leads to the second observation. Although one can construct the set of four coordinates, given in eqs 3−6, that transform under the G_1^+ irreducible representation, the calculated energies of the states that have nodes when each of these coordinates is zero are not equal. The lack of degeneracy of these states is further illustrated by the fact that each state has a different value of the participation ration, ρ, given in the fourth column of Table 3.

Before continuing to a discussion of the states that were evaluated in this study, it is useful to consider how a calculation that imposes a node based on a linear combination of CH bond lengths could produce states whose energies are too low to be CH or CD stretch fundamentals. It is also appropriate to ask whether the calculated states are relevant to a fuller understanding of the spectroscopy and dynamics of CH_5^+ and CD_5^+.

The fact that the calculated frequencies are too low to be CH or CD stretch fundamentals was, at first, surprising, but not without precedent. In our previous study of excited states of CH_5^+, we generated an excited state for which we required the wave function to change sign when $r_{12} - r_{23} = 0$, where r_{ij} represents the distance between the ith and jth hydrogen atoms.[24] Such an excited state would, at first, be thought to correspond to putting a node at the C_{2v} saddle point, shown in Figure 1a. In fact, the frequency that was obtained and the projections of

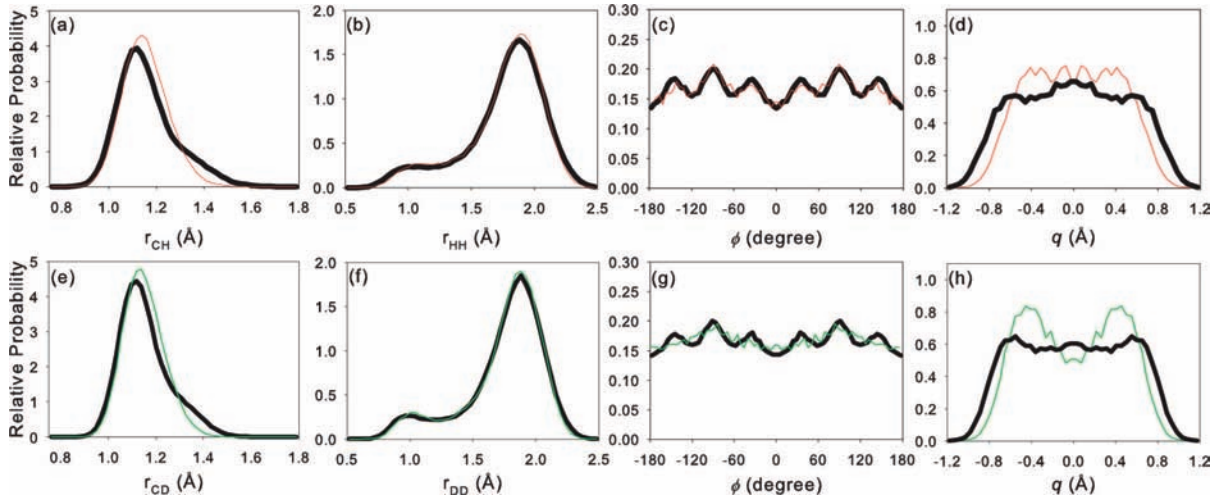

Figure 3. Projections of the probability amplitudes for the A_1^+ excited state of CH_5^+ plotted as functions of the (a) CH distance; (b) HH distance; (c) methyl rotor coordinate, ϕ; and (d) C_{2v} isomerization coordinate, q, with thick black lines. (e−h) Corresponding distributions for CD_5^+. The thin red and green lines represent the corresponding projections for the corresponding ground state.

the probability amplitude led us to conclude that the excited state contained a node at the C_s(II) saddle point, shown in Figure 1b. The difference between the expected excited state and the actual excited state that was calculated reflects the fact that the DMC simulation will provide the *lowest-energy* state that has the requisite symmetry properties. We have also encountered unexpected states in studies of Ne_2OH,[42] $H_5O_2^+$,[43] and $H_3O_2^-$.[44]

The situations we encountered in $H_5O_2^+$ and $H_3O_2^-$ are most similar to the present study. These systems can be thought of as either a pair of water molecules or hydroxide ions with an excess proton whose average position is on the OO axis, equidistant from the two oxygen atoms. In these systems, fixed-node DMC provided frequencies for the excited states that correspond to displacement of the central proton along the OO axis that were in good agreement with other calculations and experiment.[43−45] On the other hand, the frequency that corresponded to displacement of the shared proton perpendicular to the OO axis was calculated to be close to 1000 cm^{-1} in the DMC studies, whereas other approaches placed this frequency between 1300 and 1500 cm^{-1}.[43,44,46] Interestingly, the frequencies calculated from DMC corresponded to transitions in the spectra of these species, whereas little intensity is seen at the frequencies calculated by other methods. Further analysis of the DMC wave functions in combination with comparisons to states with similar energies in variational calculations led us to conclude that the DMC calculations were generating excited states that involved combination bands of lower-frequency modes. More recent multiconfigurational time-dependent Hartree calculations of $H_5O_2^+$ made similar assignments to the observed bands near 1000 cm^{-1}.[47,48]

The insights gained from these studies lead us to expect that, although the states that are evaluated in the present study are not CH stretch excitations, the identification of this set of five states provides us with an opportunity to investigate the nature of the coupling between the high- and low-frequency vibrational modes and also to obtain an initial look at rotation−vibration mixing in CH_5^+.

4.1. A_1^+ State. The excited state with A_1^+ symmetry has an energy of 2160 ± 5 cm^{-1}. This frequency is about 800 cm^{-1} lower than the value of this fundamental calculated variationally by Wang and Carrington[18] and calculated by vibrational configuration approaches by Huang et al.[6] It is also to the red of the CH stretch band in the spectrum reported by Asvany et al.[8] Consequently, we anticipate that the state we calculated is not the CH stretch fundamental, but rather a lower-energy combination band that, because of stretch/bend couplings, has the property that the wave function changes sign at a specified value of the CH distances. Although the spectrum of CD_5^+ has not been reported, a calculation of the spectrum has.[49] Again, our calculated frequency of 1551 ± 5 cm^{-1} is significantly below the calculated CD stretch fundamental band. In addition, the near factor of $1/\sqrt{2}$ between our calculated frequency and the corresponding one in CH_5^+ leads us to expect that this calculated state is also a combination band, rather than representing a fundamental in the CD stretch.

To further investigate the nature of this excited state, we plot projections of the associated probability amplitude along four internal coordinates in Figure 3. For comparison, the corresponding ground-state distributions are plotted with thin colored lines. In both CH_5^+ and CD_5^+, the projections of the probability amplitude onto r_{HH} and ϕ are not changed significantly with vibrational excitation. This fact indicates that, structurally, this excitation does not change how the molecule samples the various potential minima that are connected by the C_s(II) saddle points. On the other hand, there is an increase in the widths of the distributions when they are projected along q and the CH distance coordinates. The CH distance distribution also contains a shoulder at larger values of the CH bond lengths. The increased width is not unexpected, as the introduction of a node at a specified value of the average CH distance will necessarily increase the width of the probability amplitude when it is projected onto r_{CH}. The increase in the width of the projection of the probability amplitude onto q can be understood by the CH distances at the three stationary points, reported in Table 1. Here, we find that the value of $q_{A_1^+}$ is 0.03 Å shorter at the C_{2v} saddle point than it is at either of the other stationary points. As the distribution of CH distances that are sampled by the wave function shifts to larger values of r_{CH}, one can anticipate that there will be more probability amplitude near the C_s(I) minimum, compared to the C_{2v} saddle point, in this excited state than in the ground state. This is what is reflected in the projections, plotted in panels d and h. This effect is also seen in the shoulder in the CH distance distribution in panels a

TABLE 4: Vibrationally Averaged Rotational Constants for the Ground and Excited States of CH_5^+

state	symmetry	B_a	B_b	B_c	d_{ab}
ground	C_s(I)	3.895 ± 0.015	3.864 ± 0.021	3.848 ± 0.012	0.003 ± 0.008
	C_s(II)	3.890 ± 0.015	3.867 ± 0.018	3.851 ± 0.016	−0.001 ± 0.009
$q_{A_1^+}{}^a$	C_s(I)	3.884 ± 0.011	3.845 ± 0.010	3.832 ± 0.011	0.000 ± 0.008
	C_s(II)	3.881 ± 0.011	3.850 ± 0.011	3.831 ± 0.011	0.000 ± 0.008
$q_{G_1^+,1}$	C_s(I)	3.864 ± 0.016	3.746 ± 0.013	3.708 ± 0.014	−0.010 ± 0.007
	C_s(II)	3.865 ± 0.016	3.744 ± 0.014	3.709 ± 0.013	−0.003 ± 0.007
$q_{G_1^+,2}$	C_s(I)	4.107 ± 0.017	3.638 ± 0.013	3.575 ± 0.012	−0.056 ± 0.012
	C_s(II)	4.111 ± 0.017	3.612 ± 0.013	3.597 ± 0.013	0.038 ± 0.010
$q_{G_1^+,3}$	C_s(I)	4.084 ± 0.014	3.655 ± 0.013	3.583 ± 0.013	−0.049 ± 0.008
	C_s(II)	4.082 ± 0.014	3.632 ± 0.013	3.608 ± 0.013	0.032 ± 0.008
$q_{G_1^+,4}$	C_s(I)	3.784 ± 0.016	3.774 ± 0.015	3.759 ± 0.015	−0.006 ± 0.008
	C_s(II)	3.787 ± 0.016	3.777 ± 0.015	3.754 ± 0.015	−0.015 ± 0.007

[a] State with a node in $q_{A_1^+}$.

TABLE 5: Vibrationally Averaged Rotational Constants for the Ground and Excited States of CD_5^+

state	symmetry	B_a	B_b	B_c	d_{ab}
ground	C_s(I)	1.975 ± 0.004	1.963 ± 0.005	1.955 ± 0.006	0.000 ± 0.003
	C_s(II)	1.979 ± 0.006	1.960 ± 0.005	1.955 ± 0.006	−0.001 ± 0.004
$q_{A_1^+}{}^a$	C_s(I)	1.976 ± 0.004	1.957 ± 0.004	1.949 ± 0.004	0.000 ± 0.003
	C_s(II)	1.974 ± 0.004	1.959 ± 0.004	1.948 ± 0.004	0.000 ± 0.003
$q_{G_1^+,1}$	C_s(I)	1.973 ± 0.006	1.920 ± 0.005	1.899 ± 0.006	−0.008 ± 0.003
	C_s(II)	1.970 ± 0.006	1.920 ± 0.006	1.902 ± 0.005	−0.003 ± 0.003
$q_{G_1^+,2}$	C_s(I)	2.110 ± 0.006	1.851 ± 0.005	1.838 ± 0.005	−0.012 ± 0.003
	C_s(II)	2.100 ± 0.005	1.859 ± 0.005	1.840 ± 0.005	0.015 ± 0.003
$q_{G_1^+,3}$	C_s(I)	2.077 ± 0.005	1.881 ± 0.005	1.842 ± 0.005	−0.013 ± 0.003
	C_s(II)	2.075 ± 0.005	1.870 ± 0.005	1.855 ± 0.005	0.014 ± 0.003
$q_{G_1^+,4}$	C_s(I)	1.936 ± 0.005	1.933 ± 0.006	1.928 ± 0.005	0.004 ± 0.003
	C_s(II)	1.937 ± 0.006	1.935 ± 0.006	1.925 ± 0.005	−0.008 ± 0.003

[a] State with a node in $q_{A_1^+}$.

and e. Because of the lower vibrational frequencies in CD_5^+, the effect is even more dramatic.

To investigate coupling between this vibrational excitation and the overall rotation of the molecule, we calculate the vibrationally averaged rotational constants for CH_5^+ and CD_5^+ and compare them to the values for the ground state.[23] The results are reported in Tables 4 and 5. We find that at most four of the rotational constants are nonzero, within the statistical uncertainties of the calculations. Only these four rotational constants are reported in Tables 4 and 5. Following the notation of Ernesti and Hutson,[50] the constants represent the coefficients in

$$\hat{H}_{\text{rot}} = B_a\hat{J}_a^2 + B_b\hat{J}_b^2 + B_c\hat{J}_c^2 + d_{ab}(\hat{J}_a\hat{J}_b + \hat{J}_b\hat{J}_a) \quad (9)$$

As in the ground state, the three calculated diagonal rotational constants are nearly equal, and $d_{ab} = 0$. This indicates that this excitation does not break the rotational symmetry of CH_5^+. Upon comparison of the ground- and excited-state rotational constants, the excited-state values are slightly smaller. This is consistent with an overall extension of the average CH bond lengths, depicted in Figure 3. Analogous trends are seen for CD_5^+.

4.2. G_1^+ States. The situation is more interesting for the four excited states that correspond to excitation along the coordinates defined in eqs 3−6. Although, taken together, these four coordinates transform under the G_1^+ irreducible representation, the energies, reported in Table 3, span from 1039 to 1383 cm^{-1} in CH_5^+ and from 628 to 893 cm^{-1} in CD_5^+. In addition to not being degenerate, this range of energies spans the HCH bend region of the spectrum for CH_5^+ reported by Asvany et al.[8] and the calculated spectra for CH_5^+ and CD_5^+ reported by Huang et al.[6,49]

In Figure 4, the probability distributions are projected onto the four internal coordinates. Although these four excited states have different energies, the four projections are essentially identical to within the statistical uncertainties of the calculations. There is a small difference in the probability distribution along q for the state in which the excitation is along $q_{G_1^+,4}$. As with the excited-state distribution with A_1^+ symmetry, the distribution along the CH distance coordinate contains a shoulder at large values of r_{CH}. In addition, there is a well-defined peak near 0.98 Å in the projection along r_{HH}. This, along with the minimum in the projection of the probability amplitude along q, indicates that the nodal surfaces cross at least some of the C_{2v} saddle points, giving the excited-state wave functions more distinct CH_3^+ and H_2 subunits. In contrast, the projections of the probability amplitude along ϕ are nearly identical for the ground and excited states. The results for these four states in CD_5^+ are similar to those for CH_5^+.

Although the distributions plotted in Figure 4 clearly show coupling between each of the four $q_{G_1^+,n}$ coordinates and the coordinates that lead to isomerization, they do not explain why the four excited states have different energies. In fact, based on the similarities among these projections, one might anticipate that the four excited states could be degenerate. In contrast, the participation ratios, which provide a measure of the number of minima sampled by each of the excited states, are different and increase with increasing vibrational energy. Overall, the participation ratios for CD_5^+, reported in Table 3, are somewhat lower than those for CH_5^+. This difference reflects the smaller amplitude of the vibrations in CD_5^+, compared to those in CH_5^+.

Although the correlation between participation ratios and energy is reassuring, the trend is nonlinear. In addition, one might expect that the states that sample more minima, and

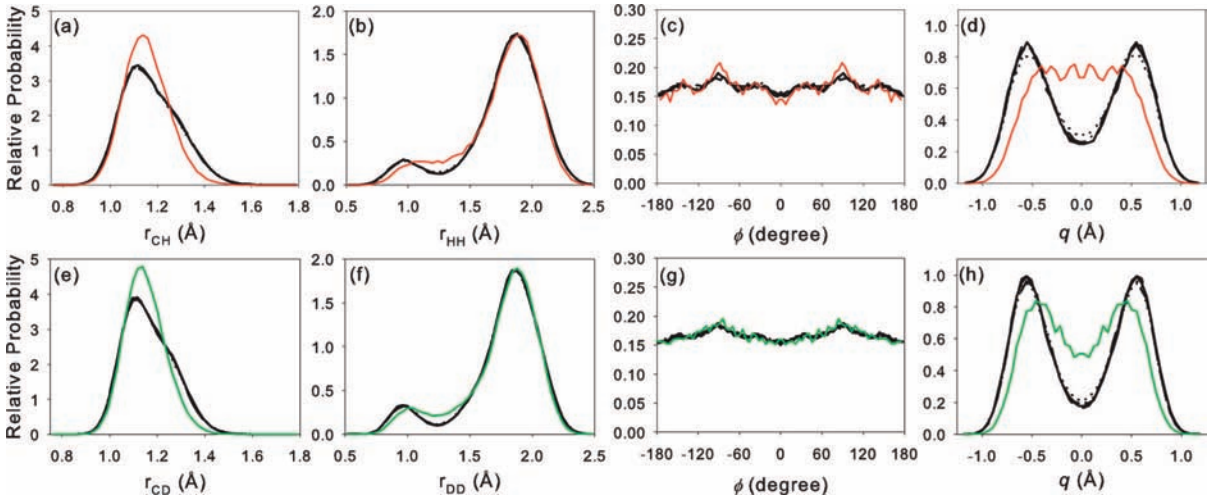

Figure 4. Projections of the probability amplitudes of the excited states of CH_5^+ with nodes in $q_{G_1^+,1}$ (solid black line), $q_{G_1^+,2}$ (dashed line), $q_{G_1^+,3}$ (dash−dot−dotted line), and $q_{G_1^+,4}$ (dotted line) plotted as functions of the (a) CH distance; (b) HH distance; (c) methyl rotor coordinate, ϕ; and (d) C_{2v} isomerization coordinate, q, with thick black lines. (e−h) Corresponding distributions for CD_5^+. The thin red and green lines represent the corresponding projections for the corresponding ground state.

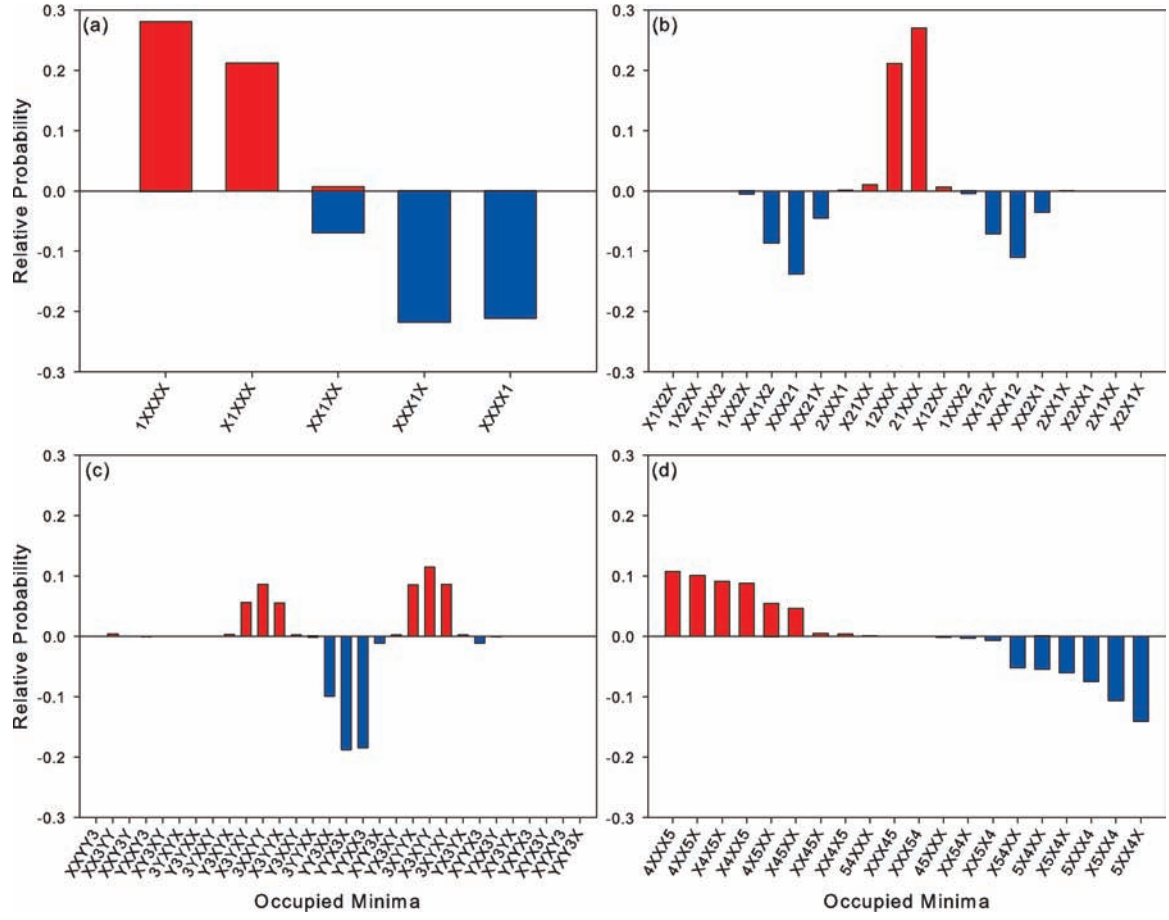

Figure 5. Projections of the probability amplitudes of the four excited states of CH_5^+ with nodes in $q_{G_1^+,n}$ onto the occupied minima, defined in Table 2. The red and blue bars provide the results of the simulations with $q_{G_1^+,n} > 0$ (red) and $q_{G_1^+,n} < 0$ (blue). Specifically, $n =$ (a) 4, (b) 3, (c) 2, and (d) 1.

consequently have larger participation ratios, would be lower in energy. In fact, the opposite trend holds for these results.

The localization of the wave function in a subset of the minima is a manifestation of couplings between the four $q_{G_1^+,n}$ coordinates and the isomerization coordinates. To understand the implications of the correlation between ρ and vibrational energy, we shift our focus to exactly which minima in the potential are sampled by the parts of the wave function with positive amplitude and which are sampled by the parts of the wave function with negative amplitude. Once we have determined this, we can map out the isomerization pathways that connect minima in a single region of space in which the wave function does not change sign. We can also examine the geometries at which the wave function changes sign.

To start, as the definition of positive and negative amplitude is arbitrary, we will equate the region of positive amplitude with

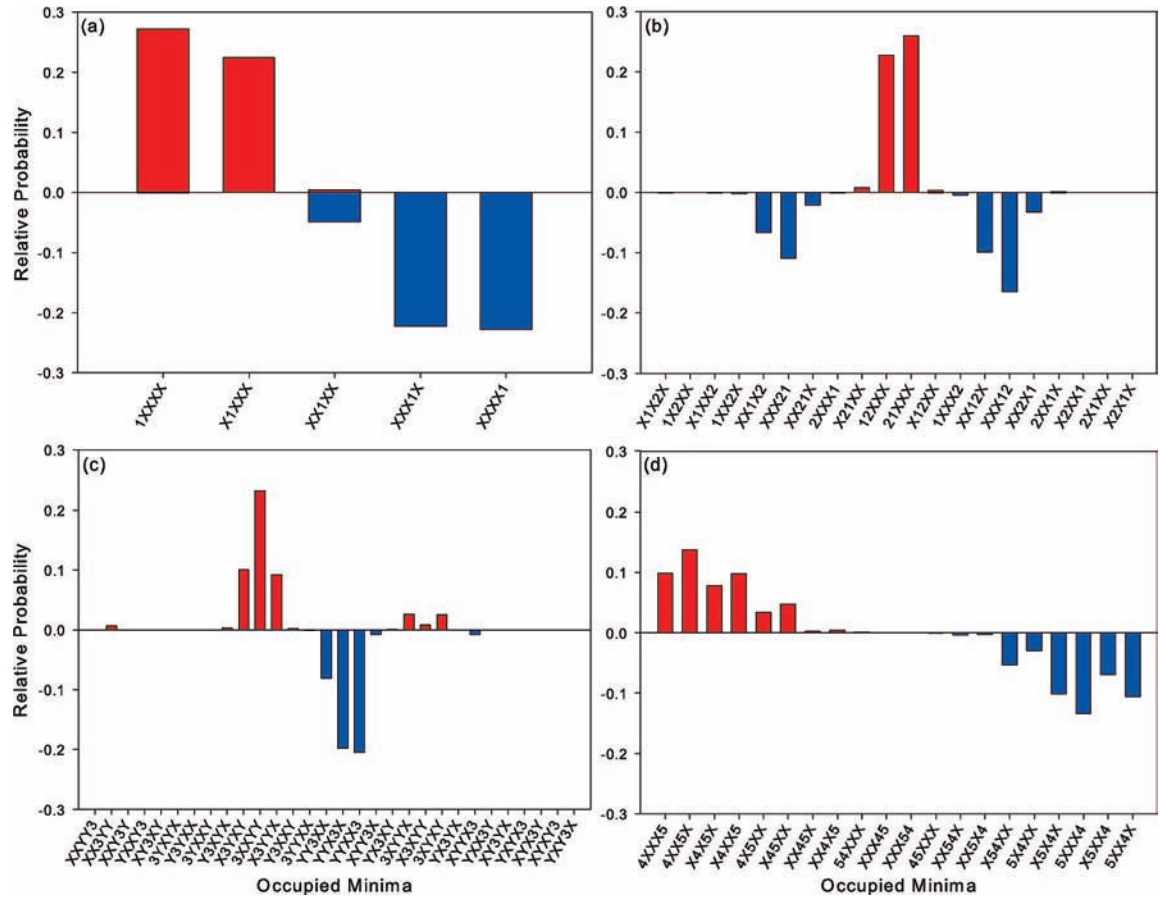

Figure 6. Projections of the probability amplitudes of the four excited states of CD_5^+ with nodes in $q_{G_1^+,n}$ onto the occupied minima, defined in Table 2. The red and blue bars provide the results of the simulations with $q_{G_1^+,n} > 0$ (red) and $q_{G_1^+,n} < 0$ (blue). Specifically, n = (a) 4, (b) 3, (c) 2, and (d) 1.

the region for which $q_{G_1^+,n} > 0$. Following the notation above, this region of space is denoted as $r_+^{(n)}$. Likewise, the region with negative amplitude, $r_-^{(n)}$, is the region for which $q_{G_1^+,n} < 0$. In Table 2, the various minima that are unique by symmetry are categorized based on whether they are in $r_+^{(n)}$ or $r_-^{(n)}$ or have amplitude that is less than 10% or 1% of the amplitude in the minimum with the greatest amplitude for that state. These results are also depicted graphically in Figures 5 and 6. When possible, the *x*-axes in these plots are arranged so that the adjacent minima are separated by a single saddle point. The exception is the state with a node in $q_{G_1^+,1}$, for which one finds that the regions with amplitude in $r_+^{(n)}$ and $r_-^{(n)}$ are separated by a long string of saddle points.

Because each of the bins in Figures 5 and 6 contains contributions from as many as 24 minima, it is hard to connect these plots directly to the localization of the wave function among the 120 equivalent minima. To further our understanding of these states, we shift our focus to the connectivity of the individual minima with population in $r_+^{(n)}$ and in $r_-^{(n)}$.

We start by considering the state with the highest energy, the one with the node in $q_{G_1^+,4}$. In this case, there is one unique hydrogen atom, labeled H_1. When $q_{G_1^+,4} > 0$, the molecule will be localized in minima in which r_1 is larger than the other CH bond lengths. Based on the geometries of the stationary points, this would correspond to minima in which H_1 is in position A or B. Likewise, when $q_{G_1^+,4} < 0$, the wave function will primarily have amplitude near the minima in which H_1 is in position D or E and, to a lesser extent, in position C. Investigation of Table 2 indicates that this is indeed the case. This result is also depicted graphically in Figure 5. Although this shows the connectivity of the minima, it does not guarantee that all 48 minima in which the wave function has positive amplitude or all 72 minima that contain negative amplitude are connected to each other through the C_s(II) or C_{2v} saddle points.

Closer examination shows that the 48 minima that are sampled in the simulation for which $q_{G_1^+,4} > 0$ divide into eight groups of six minima each. Each set of minima is connected through a set of six C_s(II) saddle points, and these groups of six minima are further connected through C_{2v} saddle points, yielding two sets of 24 connected minima. Likewise, the 72 minima that are sampled in the simulation in which $q_{G_1^+,4} < 0$ can be divided into two groups of 36 minima each. These groups of minima can be further divided into three groups of eight minima each that are separated by the 12 minima in which H_1 is in position C and the amplitude of the wave function is smaller. Taken together, the r_+ and r_- regions of space are separated by 36 of the C_{2v} saddle points, thereby explaining why the amplitude near this stationary point is lower in this excited state than in the ground state. In the end, taking into account the 96 minima with the largest amplitude, the probability amplitude for this state is divided into eight pieces, rather than two.

At the other extreme, the state with the lowest energy is the one in which the node is chosen to be in $q_{G_1^+,2}$. In this case, when $q_{G_1^+,2} > 0$, $2r_3 > r_4 + r_5$, and H_3 is preferentially located in positions A or B, with H_4 and H_5 in positions C, D, or E. Likewise, when $q_{G_1^+,2} < 0$, $2r_3 < r_4 + r_5$, and H_3 is preferentially located in position C, D, or E, with H_4 and H_5 are in positions A and B. This is seen both in the data in Table 2 and in the

plot in Figure 5. In this case, each of the reported structures represents four minima.

When the pathways connecting minima in which the wave function retains its sign are evaluated, one finds that the 32 minima with the largest amplitude in r_+ are divided into two groups of 12 that are each connected through 12 C_s(II) and 1 C_{2v} saddle points. The pathways connecting minima 12 minima with the largest amplitude in r_- are found to divide into two groups of six minima that are each connected through six C_s(II) saddle points. These four sets of minima are connected to each other through a path that contains the remaining 58 C_{2v} saddle points. In comparison to the excited state with a node in $q_{G_1^+,4}$, many fewer of the C_{2v} saddle points are expected to have probability amplitude. This is consistent with the results reported in Figure 4. Further, the wave function is subdivided into only four pieces, as compared to the eight for the state described above. This is consistent with the energy difference between these states, presented in Table 3. The remaining two excited states can be analyzed in a similar manner.

Finally, we evaluated the rotational constants for each of these states and report the results in Tables 4 and 5. When the node is placed in $q_{G_1^+,1}$ or $q_{G_1^+,4}$, the molecule retains its spherical symmetry, and d_{ab} is nearly zero. In the other two states, $B_a > B_b \approx B_c$, and $d_{ab} \neq 0$. The loss of spherical symmetry in these states can be understood by examination of Table 2. Specifically, in the states in which the node is in $q_{G_1^+,2}$ or $q_{G_1^+,3}$, two of the distinct hydrogen atoms are in positions A and B on one side of the node and in positions C, D, or E on the other. This brings the vibrationally averaged structure closer to the two C_s stationary-point structures, shown in Figure 1, with less amplitude in the region of the C_{2v} saddle point. Whereas similar behavior is seen for the other two excited states, only one of the hydrogen atoms is involved, thereby making the distortion from spherical symmetry less pronounced. Analogous behavior is seen for CD_5^+.

5. Conclusions

In this work, we investigated the wave functions for several excited states of CH_5^+. Although the initial motivation for this work was to study excited states of the stretch fundamental, the states that emerged from the calculation were somewhat lower in frequency and reflect combination bands that involve HCH bends. Four of the five states contain nodes along coordinates that, taken together, transform under the G_1^+ irreducible representation of the G_{240} permutation-inversion group. Projections of the probability amplitudes associated with these states are nearly identical, but the calculated energies differ by several hundred wavenumbers. This result was, at first, surprising. Further analysis of the wave functions showed that these four states sample the 120 minima on the CH_5^+ potential in different ways. Specifically, introducing constraints that one of the CH bond lengths must be larger or smaller than the sum of a subset of the remaining CH distances results in the wave function becoming localized in a subset of the minima on the potential. Further, the sampling of these minima is different for each of these four excited states. The structure of the nodal surface that separates the regions of space where the wave function has positive and negative amplitude is not a simple 17-dimensional function of a single coordinate, but rather a complicated function of the collective isomerization coordinates.

The consequences of this in the spectroscopy are not straightforward, as indicated by the changes in the vibrationally averaged rotational constants by as much as 10% and the reduction of the symmetry of the molecule. This reinforces the experimental observation that the rotation−vibration spectrum is complex. As we move forward, we hope to explicitly calculate rotation−vibration states with $J > 0$ directly by DMC approaches[51] in order to gain further insights into the spectroscopy and dynamics of this complicated small molecule.

Acknowledgment. Support through Grant CHE-0515627 from the Chemistry Division of the National Science Foundation is gratefully acknowledged. We also thank Professor Joel M. Bowman for providing us with the codes used to evaluate the potential used in this work. This work was supported in part by an allocation of computing resources from the Ohio Supercomputer Center.

Supporting Information Available: Character table for the G_{240} CNPI group. This material is available free of charge via the Internet at http://pubs.acs.org.

References and Notes

(1) Tal'roze, V. L.; Lyubimova, A. K. *Dokl. Akad. Nauk SSSR* **1952**, *86*, 909.
(2) Herbst, E. *J. Phys. Chem. A* **2005**, *109* (18), 4017–4029.
(3) Asvany, O.; Schlemmer, S.; Gerlich, D. *Astrophys. J.* **2004**, *617*, 685–692.
(4) Roberts, H.; Herbst, E.; Millar, T. J. *Mon. Not. R. Astron. Soc.* **2002**, *336*, 283–290.
(5) White, E. T.; Tang, J.; Oka, T. *Science* **1999**, *284*, 135–137.
(6) Huang, X.; McCoy, A. B.; Bowman, J. M.; Johnson, L. M.; Savage, C.; Dong, F.; Nesbitt, D. J. *Science* **2006**, *311*, 60–63.
(7) Savage, C.; Nesbitt, D. J. JILA, National Institute of Standards and Technology, University of Colorado, Boulder, Colorado 80309-0440, USA and Department of Chemistry and Biochemistry, University of Colorado, Boulder, Colorado 80309-0440, USA.
(8) Asvany, O.; Kumar, P.; Redlich, B.; Hegeman, I.; Schlemmer, S.; Marx, D. *Science* **2005**, *309*, 1219.
(9) Jin, Z.; Braams, B. J.; Bowman, J. M. *J. Phys. Chem. A* **2006**, *110*, 1569–1574.
(10) Kolbuszewski, M.; Bunker, P. R. *J. Chem. Phys.* **1996**, *105*, 3649–3653.
(11) East, A. L. L.; Bunker, P. R. *J. Mol. Spectrosc.* **1997**, *183*, 157–162.
(12) East, A. L. L.; Kolbuszewski, M.; Bunker, P. R. *J. Phys. Chem. A* **1997**, *101*, 6746–6752.
(13) Bunker, P. R.; Ostojic, B.; Yurchenko, S. *J. Mol. Struct.* **2004**, *695*, 253–261.
(14) Marx, D.; Parrinello, M. *Science* **1999**, *286*, 1051.
(15) McCoy, A. B.; Brown, A.; Braams, B. J.; Huang, X.; Jin, Z.; Bowman, J. M. *J. Phys. Chem. A* **2004**, *108*, 4991.
(16) Crittenden, D. L.; Thompson, K. C.; Chebib, M.; Jordan, M. J. T. *J. Chem. Phys.* **2004**, *121*, 9844–9854.
(17) Kumar, P. P.; Marx, D. *Phys. Chem. Chem. Phys.* **2006**, *8*, 573–586.
(18) Wang, X.-G.; Carrington, T., Jr. *J. Chem. Phys.* **2008**, *129*, 234102.
(19) Chittenden, D. L.; Thompson, K. C.; Chebib, M.; Jordan, M. J. T. *J. Chem. Phys.* **2004**, *121*, 9844–9854.
(20) Brown, A.; McCoy, A. B.; Braams, B. J.; Jin, Z.; Bowman, J. M. *J. Chem. Phys.* **2004**, *121*, 4105–4116.
(21) Hinkle, C. E.; McCoy, A. B.; Huang, X.; Bowman, J. M. *J. Phys. Chem. A* **2007**, *111*, 2033–2034.
(22) Marx, D.; Parrinello, M. *Science* **1999**, *284*, 59–61.
(23) Johnson, L. M.; McCoy, A. B. *J. Phys. Chem. A* **2006**, *110*, 8213–8220.
(24) Hinkle, C. E.; McCoy, A. B. *J. Phys. Chem. A* **2008**, *112*, 2058–2064.
(25) Bunker, P. R.; Jensen, P. *Molecular Symmetry and Spectroscopy*; NRC Research Press: Ottawa, Canada, 1998.
(26) Just, G. M. P.; McCoy, A. B.; Miller, T. A. *J. Chem. Phys.* **2007**, *127*, 044310/1−11.
(27) Schreiner, P. R.; Kim, S. J.; Schaefer, H. F., III.; Schleyer, P. v. R. M. *J. Chem. Phys.* **1993**, *99*, 3716–3720.
(28) Anderson, J. B. *J. Chem. Phys.* **1975**, *63*, 1499–1503.
(29) Anderson, J. B. *J. Chem. Phys.* **1976**, *65*, 4121–4127.
(30) McCoy, A. B. *Int. Rev. Phys. Chem.* **2006**, *25*, 77–108.
(31) Suhm, M. A.; Watts, R. O. *Phys. Rep.* **1991**, *204*, 293–329.
(32) Buch, V. The FritzHaber Institute for Molecular Dynamics, Hebrew University, Jerusalem 91904, Israel.

(33) Wilson, E. B.; Decius, J. C.; Cross, P. C. *Molecular Vibrations*; Dover: New York, 1955.

(34) Lee, H.-S.; Herbert, J. M.; McCoy, A. B. *J. Chem. Phys.* **1999**, *110*, 5481–5484.

(35) Lee, H.-S.; Herbert, J. M.; McCoy, A. B. *J. Chem. Phys.* **1999**, *111*, 9203–9212.

(36) Severson, M. W.; Buch, V. *J. Chem. Phys.* **1999**, *111*, 10866–10875.

(37) Coker, D. F.; Watts, R. O. *Mol. Phys.* **1986**, *58* (6), 1113–1123.

(38) Sandler, P.; Buch, V.; Sadlej, J. *J. Chem. Phys.* **1996**, *105*, 10387–10397.

(39) Bell, R. J.; Dean, P. *Faraday Discuss. Chem. Soc.* **1970**, *50*, 55–61.

(40) McCoy, A. B.; Burleigh, D. C.; Sibert, E. L. *J. Chem. Phys.* **1991**, *95*, 7449–7465.

(41) Louck, J. D.; Galbraith, H. W. *Rev. Mod. Phys.* **1976**, *48*, 69–106.

(42) Lee, H.-S.; McCoy, A. B. *J. Chem. Phys.* **2001**, *114*, 10278–10287.

(43) Hammer, N. I.; Diken, E. G.; Roscioli, J. R.; Myshakin, E. M.; Jordan, K. D.; McCoy, A. B.; Huang, X.; Carter, S.; Bowman, J. M.; Johnson, M. A. *J. Chem. Phys.* **2005**, *123*, 044308.

(44) McCoy, A. B.; Huang, X.; Carter, S.; Bowman, J. M. *J. Chem. Phys.* **2005**, *123*, 064317.

(45) Diken, E. G.; Headrick, J. M.; Roscioli, J. R.; Bopp, J. C.; Johnson, M. A.; McCoy, A. B. *J. Phys. Chem. A* **2005**, *109*, 1487–1490.

(46) McCoy, A. B.; Diken, E. D.; Johnson, M. A. *J. Phys. Chem A* **2009**, *113*.

(47) Vendrell, O.; Gatti, F.; Lauvergnat, D.; Meyer, H.-D. *J. Chem. Phys.* **2007**, *127*, 184302.

(48) Vendrell, O.; Gatti, F.; Meyer, H.-D. *J. Chem. Phys.* **2007**, *127*, 184303.

(49) Huang, X.; Johnson, L. M.; Bowman, J. M.; McCoy, A. B. *J. Am. Chem. Soc.* **2006**, *128*, 3478–3479.

(50) Ernesti, A.; Hutson, J. M. *Chem. Phys. Lett.* **1994**, *222*, 257–262.

(51) Petit, A. S.; McCoy, A. B., manuscript in preparation.

JP8112733